



Article

# Investigating the Electrical and Mechanical Properties of Polystyrene (PS)/Untreated SWCNT Nanocomposite Films

Pooyan Parnian and Alberto D'Amore \*

Department of Engineering, University of Campania "Luigi Vanvitelli", Via Roma 29, 81031 Aversa, Italy; pooyan.parnian@unicampania.it

\* Correspondence: alberto.damore@unicampania.it; Tel.: +39-081-501-0291

**Abstract:** This paper presents a study of the electrical and mechanical properties of polystyrene (PS)/carbon nanotube (CNT) composites prepared using the doctor blade technique. The nanocomposite films of PS/CNT were prepared by casting a composite solution of PS/CNT in tetrahydrofuran (THF) on a glass substrate using a doctor blade and drying in an oven. The nanocomposite films were then characterized using a tensile test and the four-point probe method to evaluate their mechanical properties and electrical conductivity. The experimental results were used to analyze the unpredicted behavior of the nanocomposite films. The experimental results showed that the electrical conductivity of the nanocomposite films became almost insensitive or unmeasurable with increasing CNT content for very dilute PS–THF solutions. In contrast, at higher PS concentrations, film conductivity increased to a given CNT threshold and then decreased. Based on PS–THF viscosity–concentration data, a discussion is elaborated that partially justifies the experimental results.

**Keywords:** polymer composite; mechanical properties; electrical conductivity; nanocomposite films



**Citation:** Parnian, P.; D'Amore, A. Investigating the Electrical and Mechanical Properties of Polystyrene (PS)/Untreated SWCNT Nanocomposite Films. *J. Compos. Sci.* **2024**, *8*, 49. <https://doi.org/10.3390/jcs8020049>

Academic Editor: Kyong Yop Rhee

Received: 3 December 2023

Revised: 28 December 2023

Accepted: 25 January 2024

Published: 29 January 2024



**Copyright:** © 2024 by the authors. Licensee MDPI, Basel, Switzerland. This article is an open access article distributed under the terms and conditions of the Creative Commons Attribution (CC BY) license (<https://creativecommons.org/licenses/by/4.0/>).

## 1. Introduction

Carbon nanotube (CNTs)-based polymers are a functional class of materials that has attracted the attention of scientists in recent years thanks to their unique and valuable properties [1–4]. Due to their inherently conductive nature, strength, and stiffness, CNTs have many applications, such as nanofillers and the reinforcement of polymers and other materials. The high length-to-diameter ratios of CNTs make them suitable for improving mechanical properties, electrical conductivity, and rheological percolations at relatively low concentrations. This aspect has opened a new path for developing a new class of composite materials for broader applications [5–7]. Moreover, CNT-based nanocomposites are very interesting for researchers because of their exceptional properties relative to their high properties-to-weight ratios [8,9].

A viable option for functional, lightweight CNT/polymer composites can be obtained by aligning CNTs in a unique direction within a polymeric matrix [10], a concept first introduced and used by Ajayan et al. [11]. They showed how remarkably the properties of whole composite materials can approach the theoretical properties of CNTs by modifying their alignment. Various techniques have been developed to include and orient CNTs in polymer matrices to obtain the desired composite properties [12]. It is believed that the fundamental understanding of their process–structure–performance relationship makes the creation of multifunctional composites with controlled hierarchical structures easier, which consequently may result in an extensive range of applications for these materials in the future [3].

The dispersion of single-walled carbon nanotubes (SWCNTs) in polymeric matrices is fundamental in enhancing composite performance by creating specific three-dimensional networks [13,14]. However, the strong  $\pi$ – $\pi$  covalent interactions between nanotubes aggregate the SWCNTs into bundles, making their dispersion challenging [15].

Generally, physical and chemical dispersion are the two main approaches to the dispersion of CNTs in polymeric matrices. Physical dispersion tries to achieve a uniform and homogeneous distribution of CNTs within the composite material without any changes in their surface chemistry. This approach can be applied through mechanical mixing, ultrasonication, or high-shear mixing to partly overcome the  $\pi$ - $\pi$  interactions between nanotubes that cause CNTs to bundle into aggregate formations [16].

Chemical dispersion is obtained by introducing functional groups on CNT surfaces and polymeric chains to increase their mutual affinity or by coating CNTs with polymers. Chemical dispersion can improve the overall performance of nanocomposite polymers by increasing the interfacial adhesion and load transfer between CNTs and the polymers [16].

Uniformly dispersing SWCNTs in polymeric solutions can be achieved via ultrasonic irradiation. CNT bundles separate and disaggregate due to the high shear stress induced by irradiation. However, the reaggregation of the separated nanotubes is still driven by  $\pi$ - $\pi$  interactions, a process that is prevented by coating the surfaces of the newly detached nanotubes with surfactant molecules [17,18]. The chemical sonication process causes an increase in the total bundle energy by increasing  $\pi$ - $\pi$  interaction distance, which is balanced by the surfactant activity that stabilizes dispersion. [19].

The uniform dispersion of CNTs increases their effectiveness and aims to achieve desired functional properties that depend on forming connected and uniformly distributed nanotube networks. For instance, the electrical conductivity of CNT/polymer nanocomposites results from direct charge transfer along the CNTs' percolation paths [20].

The minimum filler content required to create a conductive path is called the percolation threshold. The conductivity of a network increases with filler content according to a power law [20], as shown in the following equation for a model of isotropically and homogeneously distributed hard filler particles (1):

$$\sigma \propto \sigma_c (f - f_c)^t \quad (1)$$

where  $f$  is the volume fraction,  $f_c$  is the percolation threshold, and the exponent  $t$  is close to 1.94 for a three-dimensional network and 1.33 for a two-dimensional case.

When the content of filler particles drops below the critical value, the material loses its electrical conductivity and the number of paths connecting different regions  $S$  decreases very sharply by the following equation:

$$S \propto S_i (f_c - f)^{-s} \quad (2)$$

The shape of the filler particles influences the percolation threshold. SWCNTs have a lower percolation threshold in comparison to other fillers like MWCNTs, graphene oxide, and other nanofillers due to their higher aspect ratios  $A = L/d$  (the ratio of particle length to diameter) [21–24].

This study aimed to investigate the effects of polymer matrix concentration and CNT content on nanocomposite film's electrical conductivity and mechanical properties. The effect of shear force on the alignment of nanotube reinforcements was evaluated by measuring electrical conductivity and mechanical properties in the direction of applied stress. A potential application of this research could be in the production of multifunctional and high-performance filaments for additive manufacturing (AM) and, more specifically, fused filament fabrication (FFF or FDM), where 3D structures are fabricated using the deposition of melted filaments in a desired direction and pattern.

During the last few years, various methods have been proposed to prepare PS/CNT composites, such as melt blending, solution casting (doctor blade), electrospinning, and 3D printing. Among these methods, the doctor blade technique is a simple and practical method that can produce thin films of PS/CNT composites with the controlled thickness and uniformity of reinforcement agents. The doctor blade technique can induce the alignment of CNTs in PS matrices by applying shear force during the coating process. The

alignment of CNTs can enhance the anisotropic properties of the composites, such as electrical conductivity and mechanical strength along the alignment direction.

The electrical conductivity of CNT/PS composites is an important property that reveals their potential applications in flexible electronics [25], sensors and actuators [26], and biomedical devices [27], which was another objective of the current study.

Xu and Schubert [27] produced ternary composite films of polystyrene (PS), poly(*n*-alkyl methacrylate) (PAMA), and carbon nanotubes (CNTs) using the solution casting technique. They employed PAMA as a compatibilizer for the CNTs to improve their dispersion and adhesion to the PS matrix. They measured the conductivity of the nanocomposite films using the four-point probe technique, a standard method to measure a composite material's electrical conductivity according to ASTM D4496. They found that increasing the CNT content increased the conductivity, whereas conductivity decreased by increasing the PS content. They also found that the conductivity along the casting direction was higher than that in the transverse direction. They attributed this phenomenon to the alignment of CNTs in the direction of film casting due to the shear force applied during the solution casting and filmmaking processes. According to their findings, the conductivity of the PS/CNT nanocomposites ranged from  $10^{-9}$  to  $10^{-3}$  S/m for different compositions and orientations of the reinforcements inside the produced films [28].

Wang et al. [29] prepared porous foams composed of PS/CNTs using the freeze-drying technique. They used tetrahydrofuran (THF) as the solvent for PS and employed the sonication technique to disperse the CNTs physically. They poured the nanocomposite solution into a mold and let it freeze in liquid nitrogen. The frozen solvent was then sublimated under vacuum to obtain the PS/CNT foams. They measured the conductivity of the foams using the four-point probe method and realized that increasing CNT content and its alignment increased the conductivity.

They also realized that the lower density and higher porosity foams had higher conductivity due to the creation of more conductive pathways by the CNTs in the porous structure. Based on their findings, the conductivity of the PS/CNT foams could vary from  $10^{-15}$  to  $10^{-1}$  S/m for different densities and orientations of the CNTs in the foams [24].

In a similar study, Xie et al. [30] fabricated PS/CNT microstructures using direct 3D printing. A micro-extension system was used to deposit the PS/CNT composite filaments with controlled geometry and orientation onto a substrate. They found that adding more CNTs to the structure and the higher alignment of the CNTs in the structure resulted in higher conductivity. They also found that conductivity was higher for microstructures with smaller cross-section areas and longer lengths, which was attributed to the improved contact between the CNTs in the nanocomposite filaments because of higher pressure during the extrusion process. The measured conductivity in their study ranged from  $10^{-4}$  to 10 S/m for different geometries and orientations of the microstructures.

These studies have shown numerous techniques for producing PS/CNT nanocomposites, each resulting in different conductivity values due to incorporating different parameters. The better dispersion of nanotubes and, consequently, the higher electrical conductivity of nanocomposite films are highly dependent on the shear intensity applied to the nanocomposite solutions during sonication and filmmaking.

In order to achieve the highest conductivity, an optimum level of shear intensity is required to be applied to nanocomposite solutions, both by the sonication for CNT dispersion and by the doctor blade for film formation.

Min et al. [30] demonstrated that melt annealing above a polymer's glass transition temperature can produce highly electrically conductive nanocomposites. They explained that the orientation of the particles in the direction of flow, resulting from film formation, reduced the network bonding between the particles. However, after subsequent annealing, the network bonding between the particles was restored and assisted in restoring electrical conductivity paths [30].

The current study employed a two-step method to achieve the abovementioned goals: ultrasonication and thin film formation using the doctor blade technique. This approach allowed for the fabrication of PS/CNT nanocomposite thin films, possibly adjusting the films' thickness and controlling the homogeneity and uniformity of CNT dispersion. This study also tried to show the challenges in aligning CNTs in PS matrices by applying shear force during the sonication and film formation. For this purpose, different concentrations of PS and CNT were dissolved in tetrahydrofuran (THF), which served as a solvent for both the polymer and the reinforcement. The thin nanocomposite films were produced using the doctor blade technique to cast the nanocomposite solution onto a glass substrate. Then, the effects of sonication and film formation on electrical conductivity and mechanical properties were investigated [31].

## 2. Materials and Methods

### 2.1. Materials

Polystyrene (PS) powder with an average molecular weight of  $M_w \sim 350,000$  was purchased from Sigma-Aldrich (Merck, Germany). The single-walled carbon nanotubes (SWCNTs), with an outer diameter of  $1.6 \pm 0.4$  nm, a length of  $\geq 5$   $\mu\text{m}$ , a surface area of  $300$   $\text{m}^2/\text{g}$ , and a carbon nanotube content of  $\geq 80$  wt.%, were obtained from Tuball [32]. The tetrahydrofuran (THF) anhydrous ( $\geq 99.9\%$ , inhibitor-free) was purchased from Sigma-Aldrich, Merck, Darmstadt, Germany.

### 2.2. Nanocomposite Preparation

In order to produce the nanocomposite solution, different concentrations of polystyrene (PS) powder, namely 3%, 6%, and 9% by weight, were dissolved in 25 mL of tetrahydrofuran (THF) in separate glass beakers. Based on the PS concentration and weight percentage, the polymer solutions were stirred with a magnetic stirrer for 10 to 30 min to obtain a homogeneous mixture free of residual PS particles. Then, various concentrations of SWCNTs (1%, 2%, and 3 wt.% related to the weight percentage of PS) were added to the previously prepared PS-THF solutions.

In the next step, the prepared composite blends were subjected to ultrasonication for 10 min at 10 kJ of energy input using a probe sonicator to obtain a uniform and homogeneously dispersed solution of CNTs. Notably, the ultrasonication process was performed in a cold-water bath to prevent solvent evaporation due to the temperature increase caused by ultrasonic irradiation.

The composite films were fabricated using the doctor blade technique on a glass substrate to produce thin layers of films with an approximate thickness of 0.1 mm. The obtained cast nanocomposite solution was then rinsed with water, air dried, and hot pressed at  $100$   $^\circ\text{C}$  for 30 min using a laboratory scale oven to evaporate any remaining solvent from the films (Figure 1a). Samples for mechanical property characterization (80 mm  $\times$  10 mm, see Figure 1b) and electrical conductivity evaluation (50 mm  $\times$  50 mm, see Figure 1c) were cut from the composite films.

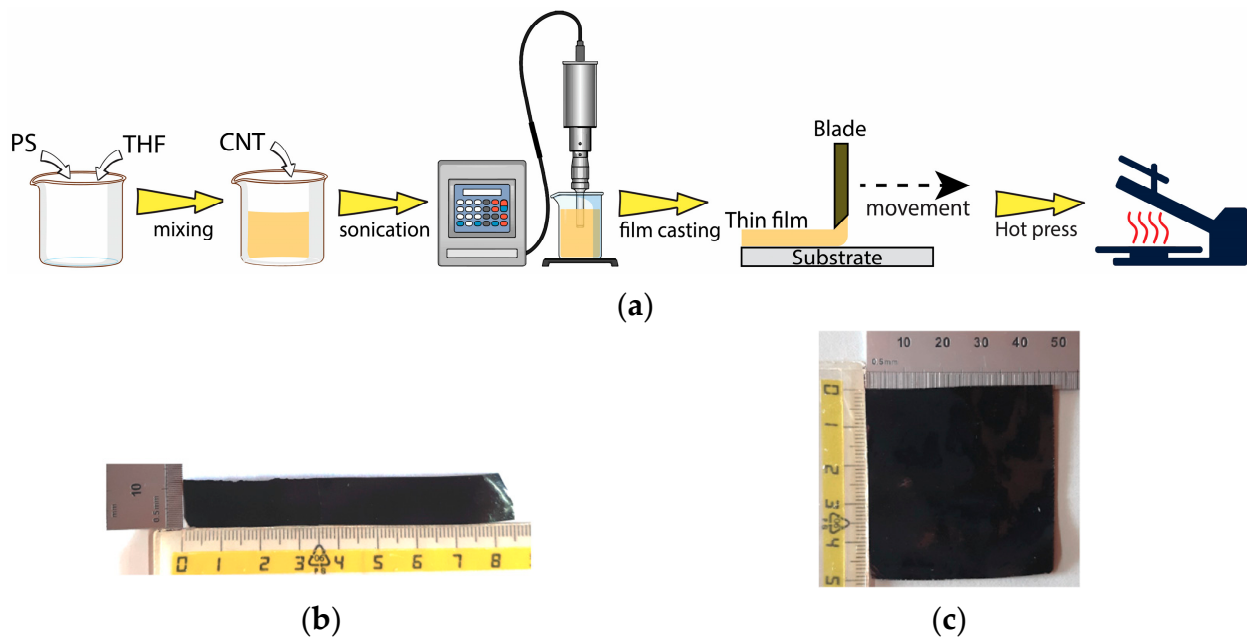


**Figure 1.** (a) Schematic of the nanocomposite film production process; (b) tensile test samples of PS/CNT nanocomposites; (c) electrical conductivity measurement test specimens.

### 2.3. Mechanical Characterization

The mechanical properties of the nanocomposite films were evaluated via tensile testing according to ASTM D882. Rectangular film specimens were tested using a ZwickRoell Z010 universal testing machine at room temperature, with a gauge length of 50 mm, a load cell of 10 kN, and a crosshead speed of 5 mm/min. The stress–strain curves resulting from the tensile testing were used to calculate the nanocomposite films’ Young’s modulus,  $E$ , and ultimate tensile strength (UTS). The reported values of  $E$  and UTS are the averages of at least four specimens for each film sample.

### 2.4. Electrical Conductivity Measurement

The four-point probe technique was employed for the electrical characterization of the nanocomposite films. Four equidistant probes were positioned linearly on each thin film, with the two outer tips facilitating current flow and the inner two tips measuring voltage. This arrangement of probes minimizes edge and contact effects and helps to measure electrical resistance precisely.

A schematic of the electrical circuit used for the conductivity measurement is presented in Figure 2. The technique is particularly suitable for small dimensional thin films, and it reduces the sample size and geometry effects.

An essential assumption in the four-point probe technique is that the thickness of a sample is much smaller than its other dimensions. Multiple measurements at different positions were taken for each sample to determine sample homogeneity and uniformity. In this regard, the electrical resistivity ( $\rho$ ) of the nanocomposite layers is written as follows:

$$\rho = R \frac{A}{L} \tag{3}$$

where  $R$  is the specimen’s electrical resistance,  $A$  is the cross-section area of the nanocomposite specimen, and  $L$  is the electrical path length. The electrical conductivity ( $\sigma$ ) can be written as follows:

$$\text{Conductivity } (\sigma, \text{S/cm}) = 1/\rho, \tag{4}$$

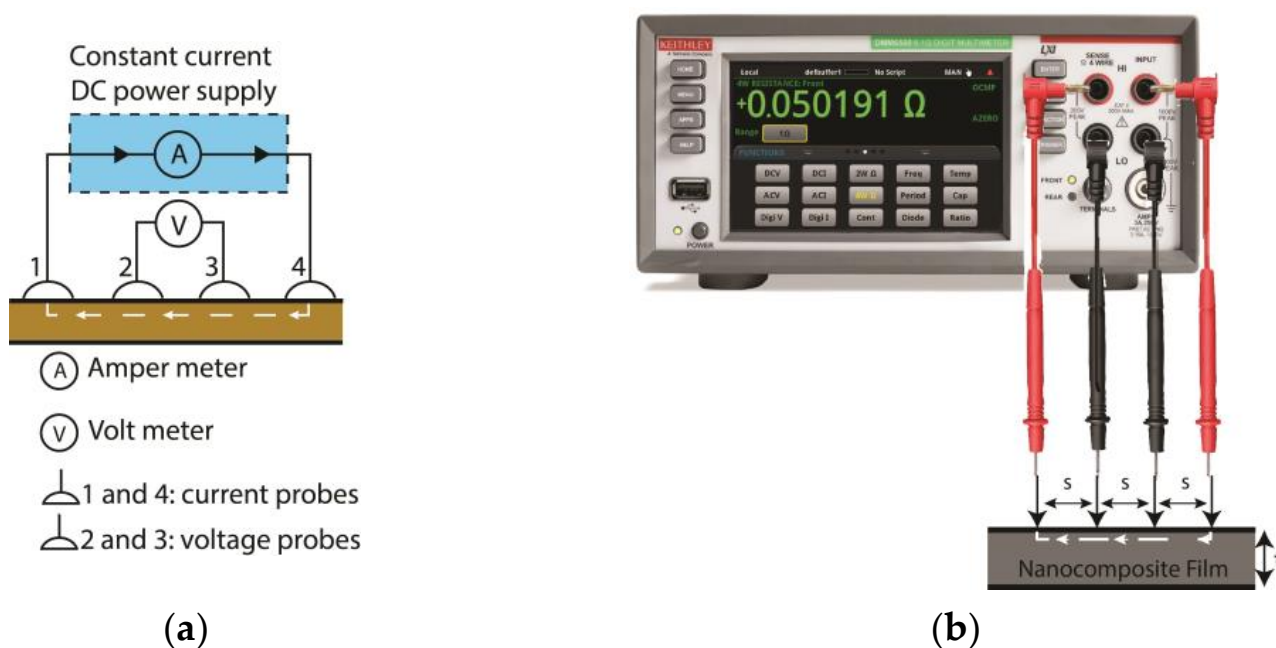


**Figure 2.** (a) Schematic of the electrical circuit used for the conductivity measurement; (b) the digital multimeter used, with a schematic of the probes used for the four-point probe technique.

### 2.5. Viscosity Measurement

An ARES-G2 TA instrument standard rheometer was used for viscosity measurements using parallel plate fixtures with a 25-mm diameter. The Newtonian viscosity was measured at 20 °C.

### 2.6. Optical Microscopy

A Zeiss AxioVert.A1 optical microscope was used to evaluate the microstructures of the cast nanocomposite thin films (as explained in Section 2.2). After preparing the nanocomposite films (Section 2.2), they were placed on a glass slide and observed with a microscope with  $\times 40$  magnification.

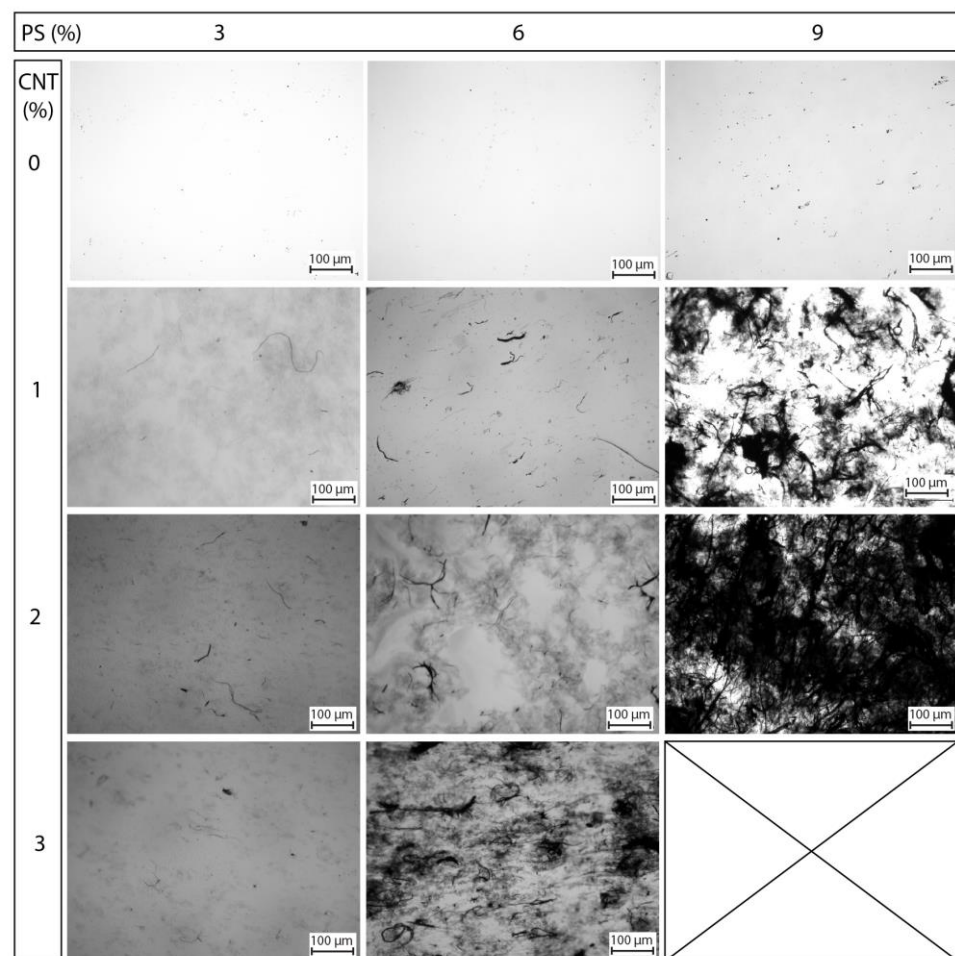
## 3. Results and Discussion

### 3.1. Microstructural Observations

In this research, 11 solutions were prepared, producing 11 thin film specimens after film casting. The second and third columns of Table 1 report the weight percentages of polystyrene (PS) that were determined relative to the volume of the solvent (25 mL THF) and the weight percentages of the carbon nanotubes (CNTs) relative to the weight of the PS, respectively. The results of the microstructural observations are summarized in Figure 3. As the PS and CNT content increased (from top to bottom and left to right), agglomerated and non-dispersed CNT bundles increased. This behavior could have been due to the higher concentrations of polymers and extra CNTs in the polymeric blends, which resulted in inhomogeneous dispersion. Precipitation and CNT agglomeration occurred for solutions containing higher concentrations of PS and CNT (the bottom right photo in Figure 3) due to the strong Van der Waals forces and  $\pi$ - $\pi$  interactions between the CNTs and their clusters [16,17].

**Table 1.** Mechanical properties of PS/CNT nanocomposite films with different content percentages.

Sample	PS (%)	CNT (%)	Young's Modulus (MPa)	UTS (MPa)
PS 3-CNT 0	3	0	2668.17	10.71
PS 3-CNT 1	3	1	1221.48	5.97
PS 3-CNT 2	3	2	3855.6	11.06
PS 3-CNT 3	3	3	709.83	4.08
PS 6-CNT 0	6	0	2189.1	47.87
PS 6-CNT 1	6	1	2917.4	17.50
PS 6-CNT 2	6	2	2778.42	10.72
PS 6-CNT 3	6	3	1384.68	4.03
PS 9-CNT 0	9	0	1464.4	17.13
PS 9-CNT 1	9	1	1441.14	8.92
PS 9-CNT 2	9	2	2496.03	6.93

**Figure 3.** Optical microscopy observations of nanocomposite films. From left to right and top to bottom, the weight percentages of PS and CNT increase.

### 3.2. Mechanical Properties

The Young's modulus,  $E$ , and ultimate tensile strength (UTS) were evaluated for each sample and the results are reported in Table 1.

Individual plots for Young's modulus and its variations are shown in Figure 4a,b to provide a more detailed understanding of the variations in mechanical properties.

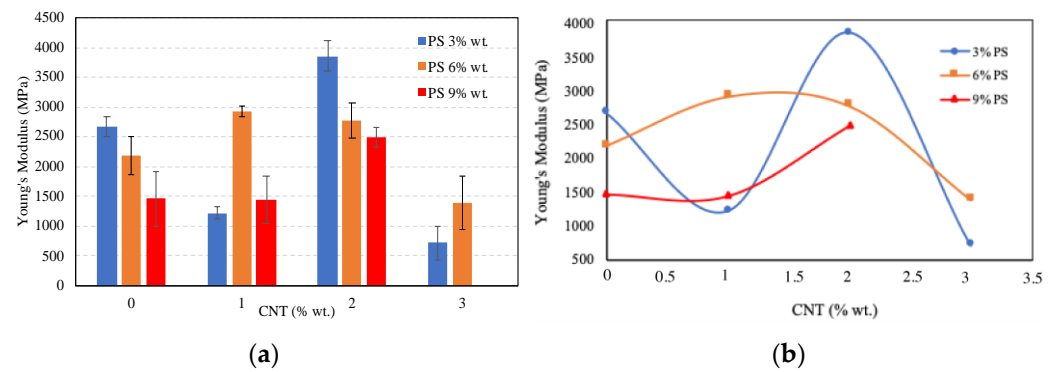


**Figure 4.** Mechanical properties of the PS/CNT nanocomposite films: (a) changes in the Young's modulus according to CNT percentages at different PS weight percentages; (b) the Young's modulus trend according to the weight percentages of CNTs for three various PS weight percentages.

As shown in Figure 4a, by increasing the content of CNT in the nanocomposite solution up to 3 wt.%, the average values of the Young's modulus decreased. The Young's modulus values of samples with 3% and 6 wt.% PS showed a maximum at roughly 1.5 and 2 wt.% CNT content. (Figure 4b). The difficulties faced in the dispersion of CNTs could be attributed to the effectiveness of sonication at higher CNT contents. It is argued that the dispersion of CNTs may depend on the actual solution viscosity, as discussed below. In samples with 2 wt.% CNT, the mechanical properties improved, as expected. However, the mechanical properties decreased above 2 wt.% CNT due to the probable clustering and agglomeration of the CNTs, which prevented efficient fiber dispersion, as shown in Figure 3.

The mechanical properties of samples containing 6 wt.% PS also increased by increasing the CNT content up to 1 wt.%. The Young's modulus values also increased, but the values were lower than those of samples with lower PS concentrations when the weight percentage of PS was increased to 9 wt.%. This behavior had consequences for the involved process variables. For example, the film formation process of highly concentrated polymer solutions at room temperature via the rapid evaporation of THF could induce the formation of a foamed structure on the nanocomposite films. The evaporation-induced film vitrification progressively raised the glass transition temperature of the solution, causing the voids left by solvent evaporation to be trapped, producing a porous structure. In addition, when increasing from 3 to 9 wt.% PS, the solvent evaporation process was considerably slowed due to the higher viscosity of the solution (a tenfold increase in viscosity, as reported in the following in Section 3.4. To verify this explanation, it can be seen from Figure 4b that the Young's modulus of the films formed from the THF/PS solution decreased by increasing the PS concentration.

The Young's modulus of films containing 3% CNT for both 3 wt.% and 6 wt.% PS decreased to less than those of pure PS films. The main reason for this could be the formation of internal fiber bundles that hindered CNT/matrix interactions. Along this line of thought, Young's modulus of samples with 9 wt.% PS increased, even when starting from lower values, because they did not pass their percolation threshold, a parameter that depends on PS concentration.

Figure 5 shows the values of tensile strain for different concentrations of CNTs. The increase in Young's modulus at any concentration of CNT, either below or above percolation (2% CNT), caused a change in the deformation behavior of the material from ductile to brittle. As a result, the increase in Young's modulus reduced the maximum tensile strain compared to pure PS.

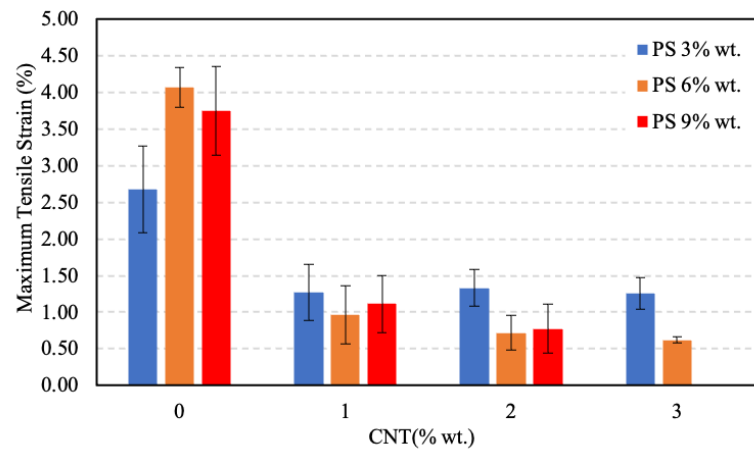


Figure 5. Maximum tensile strain values for different weight percentages of CNT and PS.

The ultimate tensile strength (UTS) results are shown in Figure 6a,b. Increasing the CNT content from 0 wt.% to 3 wt.% gradually decreased the UTS values, as already observed in the literature [16,17].

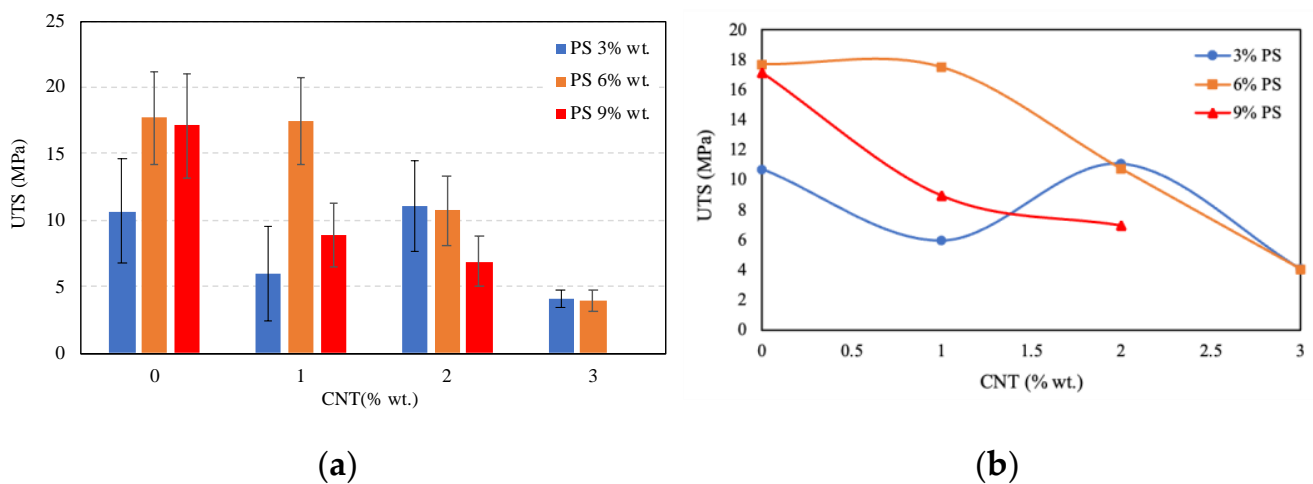


Figure 6. UTS values for various weight percentages of CNTs related to different weight percentages of PS: (a) UTS values versus CNT percentages for various weights of PS; (b) variations in the UTS values.

### 3.3. Nanocomposite Film Conductivity

In order to obtain an electrical characterization of the material that was independent of its dimensions, a measurement was carried out using the four-point probe technique. This standard technique makes it possible to measure the voltage/current ratio that produces layer resistance, assuming that the layer thickness is much smaller than the other dimensions. Theoretically, the presence of nanotubes (CNTs) in a polymer matrix provides a conductive path due to the high intrinsic electrical conductivity of the CNTs themselves. This conductive path is also called a percolating network. Therefore, higher CNT content is expected to provide more conductive pathways within nanocomposites, allowing for better electron transport and higher electrical conductivity. However, the conductivity measurement results, which are listed in Table 2, showed that there were no measurable data for some samples (notated with NA).

**Table 2.** Electrical conductivity for samples with various weight percentages of CNT and PS.

Sample	PS (%)	CNT (%)	Electrical Conductivity (S/m)
PS 3-CNT 0	3	0	0.000005
PS 3-CNT 1	3	1	0.00037037
PS 3-CNT 2	3	2	NA *
PS 3-CNT 3	3	3	0.00125
PS 6-CNT 0	6	0	NA *
PS 6-CNT 1	6	1	0.0000625
PS 6-CNT 2	6	2	$1.42857 \times 10^{-5}$
PS 6-CNT 3	6	3	0.037037037
PS 9-CNT 0	9	0	NA *
PS 9-CNT 1	9	1	0.090909091
PS 9-CNT 2	9	2	0.01369863

\* NA, no recordable results were obtained.

To better illustrate this, Figure 7 shows the conductivity values over different weight percentages of PS with increasing CNT content. In particular, this figure highlights the significantly higher conductivity of samples with higher PS content than those with lower PS concentrations.

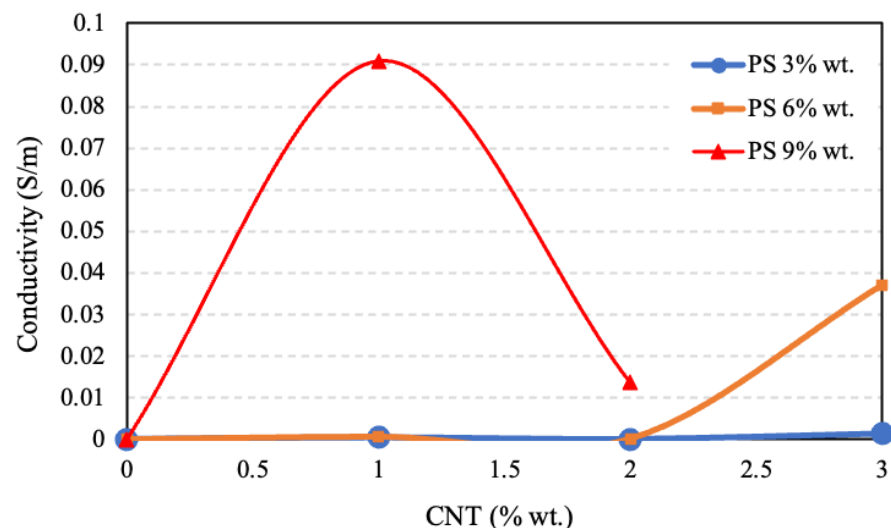


**Figure 7.** The conductivity values as a function of CNT content at different PS–THF concentrations (as indicated in the inset), measured using the four-point probe technique.

Samples with 3 wt.% PS showed no significant changes in electrical properties by increasing the weight percentage of CNT, which could have been due to the poor dispersion of the CNTs in the polymeric matrices. The inadequate and inhomogeneous dispersion of CNTs in a matrix can result in clusters or voids that disrupt conductive pathways. As a result, the measurement of electrical conductivity can be challenging [18,19].

By increasing the CNT content in samples containing 6 wt.% PS did not improve electrical conductivity until a percolation threshold was reached at 2 wt.%. As a result, electrical conductivity after this threshold increased significantly and reached about 0.037 S/m at a 3 wt.% CNT content due to the formation of electrical pathways within the nanocomposite films, as has been reported in other references [20].

Samples containing 9 wt.% PS experienced a considerable increase in electrical conductivity after adding only 1 wt.% of CNT to the pure polymer. A possible explanation for the subsequent decreases in electrical properties at higher CNT content could be that the CNTs clustered after adding more reinforcements. Notably, the efficiency of sonication in dispersing CNTs may be reduced due to higher viscosity suspensions, as discussed below.

### 3.4. Solution Viscosity Effects

The results discussed so far were challenging to interpret, even though some were consistent with physical expectations. Several factors can influence the dispersion of CNTs and their mechanical and electrical properties. The effect of polymer solution viscosity, among other factors, has been studied. Jakuba et al. [33] found that increasing the number of nanotubes altered the selectivity and dispersion of higher molecular weight polymers. Taking into account the different effectiveness of the solvents, they proposed that solution viscosity was one of the factors influencing the apparent selectivity by changing the re-aggregation rate of the single-walled carbon nanotubes (SWCNTs). Thus, the type of solvent, polymer molecular weight, concentration, and viscosity should be taken into account when screening for new polymers for selective SWNT dispersion.

Polymer solution viscosity is a function of polymer concentration and molecular weight. Figure 8 reports the experimental data for solution viscosity as a function of polymer concentration. For the case under study, the polymer molecular weight was fixed. Owing to the viscoelastic nature of the polymer solutions, we measured the “zero shear” solution viscosity,  $\eta_0$ , which is referred to as Newtonian viscosity, to distinguish it from shear rate-dependent values. In abscissa, the polymer weight percentage was converted into a concentration  $c$  ( $\text{g}/\text{cm}^3$ ), considering the density of THF ( $\rho = 0.888 \text{ g}/\text{cm}^3$ ). The viscosity of THF was  $\eta_s = 0.46 \text{ mPa}\cdot\text{s}$  and the theoretical  $\eta_0$  data as a function of polymer concentration  $c$  were also compared to those reported in [34,35] for PS solutions with different molecular weights and solvents.

Theoretically, given the polymer molecular weight, it is observed that:

$$\begin{aligned} \eta_0 &= K * c^\alpha \text{ for } c < c^* \\ \eta_0 &= K' * c^\beta \text{ for } c > c^* \end{aligned} \quad (5)$$

where  $K$  and  $K'$  are constants, depending on polymer/solvent system. The concentration exponents  $\alpha$  and  $\beta$  define the dilute and concentrated behavior of the polymer solution and  $c^*$  is the concentration at which chain entanglements become effective. Once chains are close enough to become entangled, the flow becomes much more difficult because forces applied to one polymer chain are transmitted to and distributed among many other chains. The theoretical value of the exponent  $\beta = 3.4$  is predicted using the tube model (reptation concept) [36] on polymer solutions at a constant concentration as a function of polymer molecular weight. Similar behavior was expected in our study, where the molecular weights remained fixed. The exponent appeared to be somewhat higher than 3.4 for  $c > c^*$ , a result that compared well to other results [34,35]. In dilute solutions, macromolecules are dispersed when  $c < c^*$  and weakly interact ( $\alpha < 1$ ).

Thus, the critical concentration  $c^*$  is a turning point defining the two limiting viscosity domains. In Figure 8, the asymptotic straight lines, drawn as guides, represent the two regimes below and above the critical concentration  $c^*$ . Also, Figure 8 shows that the solution concentrations adopted in the present study were close to the critical concentration  $c^*$ . However, viscosity varied smoothly over a relatively narrow range in concentration, a clear indication of the intermediate viscosity domain, which justified, at least in part, our results. We argue that polymer concentrations near the critical concentration prevented the formation of stable network structures of CNTs in the systems under study.

From a different viewpoint, let us consider that by increasing PS concentration above its critical value, viscosity raised several orders of magnitude and eventually matched the viscosity range of PS in the melt state. In this regard, Mitchell et al. [36] added functionalized single-wall carbon nanotubes (SWCNTs) to PS, studied the melt rheology of the nanocomposites, and demonstrated the formation of hydrodynamically percolated filler network structures accompanied by the development of finite yield stress at SWCNT concentrations exceeding 1.5 wt.%. In contrast, the unfunctionalized SWCNT-based hybrids exhibited no percolated structures, even at 3 wt.% SWCNT. This result was consistent with

the weak and unstable nanotube dispersion shown in the present study, including the behavior of the 9 wt.% PS solution.

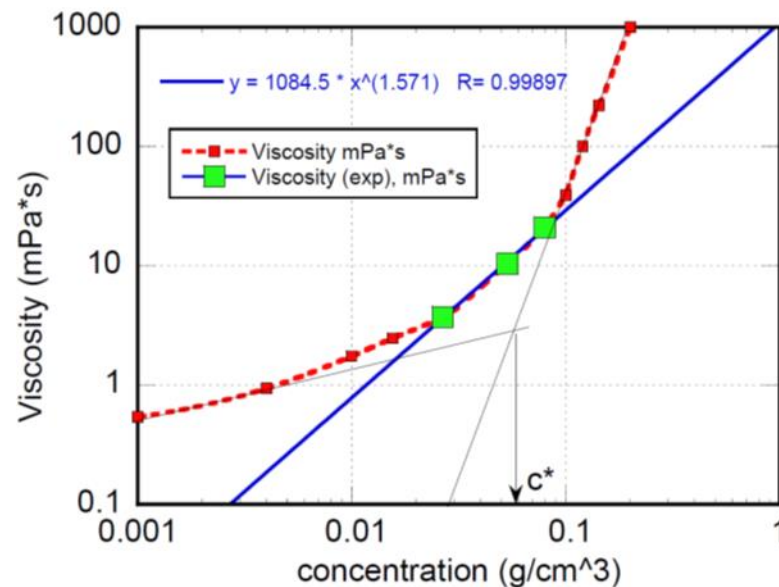


**Figure 8.** The “zero shear” viscosity of PS–THF solutions as a function of polymer concentration. The green symbols highlight the concentrations and viscosity domains of the solutions used for CNT dispersions in this study. The blue line is a guide.

#### 4. Conclusions

This study investigated the effects of polystyrene (PS) and unmodified carbon nanotube (CNT) content on the electrical and mechanical properties of nanocomposite films produced using the doctor blade technique. The nanocomposite films were prepared by coating a PS/CNT solution in tetrahydrofuran (THF) on a glass substrate using a fixed gap doctor blade and drying them in an oven. The four-point probe technique was used to measure the films’ electrical conductivity, and their mechanical strength was evaluated via tensile testing. The results showed that film electrical conductivity and mechanical strength increased by increasing CNT content to a specific threshold. This finding suggests that the PS/CNT composites can be tuned for various applications by adjusting the PS and CNT contents. Overall, the rheological behavior of CNT/polymer solutions has a relevant role in the stability and performance of the produced nanocomposite films.

**Author Contributions:** Investigation and original draft preparation, P.P.; methodology, validation, and conceptualization, A.D. All authors have read and agreed to the published version of the manuscript.

**Funding:** This research received no external funding.

**Institutional Review Board Statement:** Not applicable.

**Informed Consent Statement:** Not applicable.

**Data Availability Statement:** Data are contained within the article.

**Conflicts of Interest:** The authors declare no conflicts of interest.

#### References

1. Kavinkumar, T.; Manivannan, S. Thermal and dielectric properties of multi-walled carbon nanotube–graphene oxide composite. *J. Mater. Sci. Mater. Electron.* **2017**, *28*, 344–353. [[CrossRef](#)]
2. Xu, H.; Song, G.; Zhang, L.; Zhao, Z.; Liu, Z.; Du, T.; Song, J.; Yang, Y.; Cheng, Y.; Wei, Y.; et al. Preparation and performance evolution of enhancement polystyrene composites with graphene oxide/carbon nanotube hybrid aerogel: Mechanical properties, electrical and thermal conductivity. *Polym. Test.* **2021**, *101*, 107283. [[CrossRef](#)]

3. Goh, P.S.; Ismail, A.F.; Ng, B.C. Directional alignment of carbon nanotubes in polymer matrices: Contemporary approaches and future advances. *Compos. Part A Appl. Sci. Manuf.* **2014**, *56*, 103–126. [[CrossRef](#)]
4. Parnian, P. A Short Review on: Recent Advances in the Use of Carbon Nanotubes in Additive Manufacturing of Polymer Matrix Composites. *Macromol. Symp.* **2022**, *405*, 2100339. [[CrossRef](#)]
5. Meincke, O.; Kaempfer, D.; Weickmann, H.; Friedrich, C.; Vathauer, M.; Warth, H. Mechanical properties and electrical conductivity of carbon-nanotube filled polyamide-6 and its blends with acrylonitrile/butadiene/styrene. *Polymer* **2004**, *45*, 739–748. [[CrossRef](#)]
6. Shi, X.; Hudson, J.L.; Spicer, P.P.; Tour, J.M.; Krishnamoorti, R.; Mikos, A.G. Rheological behaviour and mechanical characterization of injectable poly (propylene fumarate)/single-walled carbon nanotube composites for bone tissue engineering. *Nanotechnology* **2005**, *16*, S531. [[CrossRef](#)] [[PubMed](#)]
7. Sung, Y.T.; Han, M.S.; Song, K.H.; Jung, J.W.; Lee, H.S.; Kum, C.K.; Joo, J.; Kim, W.N.; Kim, W.N. Rheological and electrical properties of polycarbonate/multi-walled carbon nanotube composites. *Polymer* **2006**, *47*, 4434–4439. [[CrossRef](#)]
8. Breuer, O.; Sundararaj, U. Big returns from small fibers: A review of polymer/carbon nanotube composites. *Polym. Compos.* **2004**, *25*, 630–645. [[CrossRef](#)]
9. Parihar, S.; Gaur, B. High-performance self-healing polymeric nanocomposite coatings. *Prog. Org. Coat.* **2023**, *182*, 107626. [[CrossRef](#)]
10. Ajayan, P.M.; Stephan, O.; Colliex, C.; Trauth, D. Aligned carbon nanotube arrays formed by cutting a polymer resin—Nanotube composite. *Science* **1994**, *265*, 1212–1214. [[CrossRef](#)] [[PubMed](#)]
11. Jung, Y.J.; Kar, S.; Talapatra, S.; Soldano, C.; Viswanathan, G.; Li, X.; Yao, Z.; Qu, F.S.; Avadhanula, A.; Vajtai, R.; et al. Aligned carbon nanotube—polymer hybrid architectures for diverse flexible electronic applications. *Nano Lett.* **2006**, *6*, 413–418. [[CrossRef](#)] [[PubMed](#)]
12. Pramanik, C.; Gissinger, J.R.; Kumar, S.; Heinz, H. Carbon nanotube dispersion in solvents and polymer solutions: Mechanisms, assembly, and preferences. *ACS Nano* **2017**, *11*, 12805–12816. [[CrossRef](#)]
13. Monthieux, M.; Smith, B.W.; Burteaux, B.; Claye, A.; Fischer, J.E.; Luzzi, D.E. Sensitivity of single-wall carbon nanotubes to chemical processing: An electron microscopy investigation. *Carbon* **2011**, *39*, 1251–1272. [[CrossRef](#)]
14. Predtechenskiy, M.R.; Khasin, A.A.; Smirnov, S.N.; Bezrodny, A.E.; Bobrenok, O.F.; Dubov, D.Y.; Kosolapov, A.G.; Lyamysheva, E.G.; Muradyan, V.E.; Saik, V.O.; et al. New Perspectives in SWCNT Applications: Tuball SWCNTs. Part 2. New Composite Materials through Augmentation with Tuball. *Carbon Trends* **2022**, *8*, 100176. [[CrossRef](#)]
15. Ma, P.C.; Siddiqui, N.A.; Marom, G.; Kim, J.K. Dispersion and functionalization of carbon nanotubes for polymer-based nanocomposites: A review. *Compos. Part A Appl. Sci. Manuf.* **2010**, *41*, 1345–1367. [[CrossRef](#)]
16. Rennhofer, H.; Zanghellini, B. Dispersion state and damage of carbon nanotubes and carbon nanofibers by ultrasonic dispersion: A review. *Nanomaterials* **2021**, *11*, 1469. [[CrossRef](#)] [[PubMed](#)]
17. Eskandari, P.; Abousalman-Rezvani, Z.; Roghani-Mamaqani, H.; Salami-Kalajahi, M. Polymer-functionalization of carbon nanotube by in situ conventional and controlled radical polymerizations. *Adv. Colloid Interface Sci.* **2021**, *294*, 102471. [[CrossRef](#)]
18. Fujigaya, T.; Nakashima, N. Non-covalent polymer wrapping of carbon nanotubes and the role of wrapped polymers as functional dispersants. *Sci. Technol. Adv. Mater.* **2015**, *16*, 024802. [[CrossRef](#)]
19. Alsharif, J.M.; Taha, M.R.; Khan, T.A. Physical dispersion of nanocarbons in composites—A review. *J. Teknol.* **2017**, *79*, 69–81. [[CrossRef](#)]
20. Razavi, S.M.; Sadollah, A.; Al-Shamiri, A.K. Prediction and optimization of electrical conductivity for polymer-based composites using design of experiment and artificial neural networks. *Neural. Comput. Appl.* **2022**, *34*, 7653–7671. [[CrossRef](#)]
21. Folorunso, O.; Hamam, Y.; Sadiku, R.; Ray, S.S.; Joseph, A.G. Parametric analysis of electrical conductivity of polymer-composites. *Polymers* **2019**, *11*, 1250. [[CrossRef](#)] [[PubMed](#)]
22. Schuetze, A.P.; Lewis, W.; Brown, C.; Geerts, W.J. A laboratory on the four-point probe technique. *Am. J. Phys.* **2004**, *72*, 149–153. [[CrossRef](#)]
23. Mylsamy, G.; Krishnasamy, P. A Review on Electrical Properties of Fiber-Reinforced Polymer Material: Fabrication, Measurement, and Performances. *Trans. Indian Inst. Met.* **2023**, *76*, 1–18. [[CrossRef](#)]
24. Xie, Y.; Li, Z.; Tang, J.; Li, P.; Chen, W.; Liu, P.; Li, L.; Zheng, Z. Microwave-assisted foaming and sintering to prepare lightweight high-strength polystyrene/carbon nanotube composite foams with an ultralow percolation threshold. *J. Mater. Chem. C* **2021**, *9*, 9702–9711. [[CrossRef](#)]
25. Khan, M.U.; Gomes, V.G.; Farahani, T.D. Polymer nanocomposite synthesis via ‘in-situ’ emulsion polymerization for sensor application. *Chemeca* **2011**, *2011*, 2533–2542.
26. Kausar, A.; Rafique, I.; Muhammad, B. Significance of carbon nanotube in flame-retardant polymer/CNT composite: A review. *Polym. Plast. Technol. Eng.* **2017**, *56*, 470–487. [[CrossRef](#)]
27. Xu, H.; Schubert, D.W. Electrical conductivity of polystyrene/poly (n-alkyl methacrylate) s/carbon nanotube ternary composite casting films. *J. Polym. Res.* **2020**, *27*, 153. [[CrossRef](#)]
28. Zeimaran, E.; Akbarivakilabadi, A.; Majumder, M. Polystyrene carbon nanotube nanocomposites. *Handbook of Polymer Nanocomposites. Process. Perform. Appl. Vol. B Carbon Nanotub. Based Polym. Compos.* **2015**, 213–244. [[CrossRef](#)]

29. Wang, S.; Huang, Y.; Chang, E.; Zhao, C.; Ameli, A.; Naguib, H.E.; Park, C.B. Evaluation and modeling of electrical conductivity in conductive polymer nanocomposite foams with multiwalled carbon nanotube networks. *Chem. Eng. J.* **2021**, *411*, 128382. [[CrossRef](#)]
30. Min, C.; Shen, X.; Shi, Z.; Chen, L.; Xu, Z. The electrical properties and conducting mechanisms of carbon nanotube/polymer nanocomposites: A review. *Polym. Plast. Technol. Eng.* **2010**, *49*, 1172–1181. [[CrossRef](#)]
31. Tuball Graphene Nanotubes. Available online: <https://tuball.com/about-tuball> (accessed on 25 December 2023).
32. Jakubka, F.; Schießl, S.P.; Martin, S.; Englert, J.M.; Hauke, F.; Hirsch, A.; Zaumseil, J. Effect of Polymer Molecular Weight and Solution Parameters on Selective Dispersion of Single-Walled Carbon Nanotubes. *ACS Macro Lett.* **2012**, *1*, 815–819. [[CrossRef](#)] [[PubMed](#)]
33. Kulicke, W.-M.; Kniewske, R. The shear viscosity dependence on concentration, molecular weight, and shear rate of polystyrene solutions. *Rheol. Acta* **1984**, *23*, 75–83. [[CrossRef](#)]
34. Hwang, J.-Y.; Nish, A.; Doig, J.; Douven, S.; Chen, C.-W.; Chen, L.-C.; Nicholas, R.J. Polymer Structure and Solvent Effects on the Selective Dispersion of Single-Walled Carbon Nanotubes. *J. Am. Chem. Soc.* **2008**, *130*, 3543–3553. [[CrossRef](#)]
35. Osaki, K.; Kurata, M. Experimental Appraisal of the Doi-Edwards Theory for Polymer Rheology Based on the Data for Polystyrene Solutions. *Macromolecules* **1980**, *13*, 671–676. [[CrossRef](#)]
36. Mitchell, C.A.; Bahr, J.L.; Arepalli, S.; Tour, J.M.; Krishnamoorti, R. Dispersion of Functionalized Carbon Nanotubes in Polystyrene. *Macromolecules* **2002**, *35*, 8825–8830. [[CrossRef](#)]

**Disclaimer/Publisher’s Note:** The statements, opinions and data contained in all publications are solely those of the individual author(s) and contributor(s) and not of MDPI and/or the editor(s). MDPI and/or the editor(s) disclaim responsibility for any injury to people or property resulting from any ideas, methods, instructions or products referred to in the content.